Journal of Membrane Science 611 (2020) 118273

Contents lists available at ScienceDirect

Journal of Membrane Science

journal homepage: http://www.elsevier.com/locate/memsci

Carbon nanotube-supported polyamide membrane with minimized internal concentration polarization for both aqueous and organic solvent forward osmosis process

Zongyao Zhou [a,b], Yunxia Hu [a,*], Qun Wang [a], Baoxia Mi [c]

[a] State Key Laboratory of Separation Membranes and Membrane Processes, National Center for International Research on Membrane Science and Technology, School of Materials Science and Engineering, Tianjin Polytechnic University, Tianjin, 300387, PR China
[b] CAS Key Laboratory of Coastal Environmental Processes and Ecological Remediation, Yantai Institute of Coastal Zone Research, Chinese Academy of Sciences, Yantai, 264003, PR China
[c] Department of Civil and Environmental Engineering, University of California, Berkeley, CA, 94720, United States

ARTICLE INFO

Keywords:
Carbon nanotube
Organic solvent recovery
Forward osmosis
Membrane
Polyamide

ABSTRACT

We proposed a novel strategy for fabricating a high-performance forward osmosis (FO) membrane by forming a polyamide (PA) selective layer via interfacial polymerization on top of an interconnected porous carbon nanotube (CNT) network support. The fabricated CNT-PA membrane had a highly permeable and selective PA layer for fast water and solvents passage with efficient salt and solutes rejection, and an ultrathin CNT support that significantly reduced the internal concentration polarization in the FO process. Tested in the FO (e.g., active layer facing feed solution) mode using DI water as feed solution and 1.0 M NaCl as draw solution, the optimal CNT-PA membrane exhibited a water flux of as high as 139 L m^{-2} h^{-1}(LMH)with comparable salt rejection, 686% higher than that of commercial FO membrane, outperforming the previously reported best FO membranes tested under similar conditions. Besides, the CNT-PA membrane also showed great capability to recover organic solvents such as ethanol (EtOH), dimethylsulfoxide (DMSO), dimethylformamide (DMF) and dimethylacetamide (DMAc) when used in the organic solvent forward osmosis (OSFO) process and to concentrate chemicals in organic solvents. Results present that the CNT-PA membrane exhibited a DMAc flux of around 20 LMH with near 100% rhodamine B dye rejection and a negligible reverse solute flux when using 2.0 M PEG400 as a draw solution. The contributions of the CNT support layer and the PA selective layer to the osmotic filtration performance of the CNT-PA membrane were investigated and discussed to provide insights on the FO membrane design and fabrication for the efficient separation in aqueous and organic solvent system.

1. Introduction

Forward osmosis (FO) is an emerging advanced membrane process operated under no/low hydraulic pressure and has been widely used as an efficient approach to desalinate hypersaline water [1–5], concentrate products [6–8], treat wastewater [9,10], and others in aqueous solutions [11–15]. Unlike other pressure-driven membrane processes, FO exhibits several characteristics of advantages including lower fouling tendency and higher flux recovery [14,16–18]. Besides, FO is expected to work efficiently in the separations where the osmotic pressure of target solution is too high to be operated in the pressure-driven membrane processes [11].

Very recently, the organic solvent forward osmosis (OSFO) process has been firstly demonstrated to separate chemicals from organic solvents, which shows the great application potential of FO process in chemical separation involving organic solvents [12]. However, the solvent flux of the OSFO membrane used in the work has been limited to 2.65 L m^{-2} h^{-1} (LMH), even at very high concentration of draw solution (2.0 M LiCl in Ethanol) with the osmotic pressure difference of ~50 bar. This is because the thick polymeric support of the thin-film-composite (TFC) membrane aggravates the internal concentration polarization (ICP) and limit the flux [12]. To further promote the real application of the OSFO, high-flux FO membranes with less ICP are greatly desired for the efficient OSFO process.

The ICP is widely reported coming from tortuous the support layer of the TFC polyamide (PA) membrane due to its poor porosity, high

* Corresponding author.
E-mail address: yunxiahu@yic.ac.cn (Y. Hu).

https://doi.org/10.1016/j.memsci.2020.118273
Received 12 December 2019; Received in revised form 11 May 2020; Accepted 14 May 2020
Available online 29 May 2020

tortuosity and its thickness [5,19–21]. Conventional TFC FO membranes cannot further increase their flux under the increasing driving force at higher concentrations of draw solution due to the ICP [22–25]. Therefore, the rational design and fabrication of porous supports is a key to minimize the ICP problem and thus to improve the performance of FO membranes. The ideal support of TFC FO membrane should have open porous structure with small thickness and low tortuosity providing a short path for draw solute to diffuse out and thus to suppress the ICP [26–30]. An electrospun polyethersulfone nanofibrous support has been developed as a unique, scaffold-like, interconnected porous structure providing direct paths for salt diffusion and water permeation in the FO process, and its structural parameter was less than 100 μm, while its water flux was approximately 50 LMH [23]. Although significant improvement has been made to decreasing ICP and improving the performance of the TFC FO membrane, the electrospun nanofibrous polymeric support was not solvent resistant to be used in OSFO operation.

Undoubtedly, designing a nanofibrous-like support with solvent resistant materials is a perfect strategy to obtain OSFO membranes with less ICP and strong solvent resistant, simultaneously. Hence, in this work, we fabricated a high performance OSFO membrane with a PA selective layer and an ultrathin carbon nanotubes (CNT) network support, which are both typical solvent resistant materials. First, the fully porous CNT support results in the significant mitigation of ICP and thus the significant increase of organic solvent flux. Second, the smooth CNT support with favorable hydrophilic surface provided a favorable interface for interfacial polymerization then forming a high-performance PA layer. Besides, to better investigate and evaluate the FO performance and ICP effect, the water permeability and salt rejection of the fabricated membranes were further measured. As a result, the optimal membrane exhibited a water flux of as high as 150 LMH with comparable salt rejection, and an ultra-low structural parameter of 38 μm, outperforming all existing commercial FO membranes and previously reported best FO membranes to the best of our knowledge. More importantly, we evaluated the OSFO process for solvent recovery. The resulting OSFO membrane exhibited a super-high DMAc solvent flux over 20 LMH while maintaining a near 100% solute rejection and required no external pressure. In addition, the prepared OSFO membrane exhibited excellent permeability and resistance to ethyl alcohol (EtOH), dimethylsulfoxide (DMSO) and dimethylformamide (DMF). Our research supplies a high-flux CNT supported PA membrane with significantly suppressed ICP for the recovery of pure water and organic solvents as well as the concentration of salts and chemicals in aqueous and organic solvent FO process, respectively.

2. Experimental

Materials: CNT powder (less than 2 nm in diameter, 5–30 μm in length, with a purity of over 95%), m-phenylenediamine (MPD, >99%) and tris buffer (0.1 M, pH = 7.5) were purchased from Aladdin Biochemical Technology Co., Ltd. (Shanghai, China). Trimesoyl chloride (TMC, 98%) was purchased from J&K Scientific Ltd. (Beijing, China). Dopamine hydrochloride was purchased from Sigma-Aldrich (St. Louis, MO, USA). PES microfiltration membrane (with 0.22 μm pore size) was obtained from Yibo Co. Ltd. (Haining, China). Rhodamine B was obtained from Kermel Chemical Reagent Co. Ltd. Ethyl alcohol (EtOH), dimethylsulfoxide (DMSO), dimethylformamide (DMF) and dimethylacetamide (DMAc) were obtained from Sinopharm Chemical Reagent Co., Ltd. (Beijing, China) and used as received.

Preparation of polydopamine (PDA)-coated carbon nanotube (CNT) dispersion: The CNT dispersion was prepared by sonicating CNT powder in water using a reported protocol [31]. Specifically, first, 10 mg CNT was dissolved in 100 mL DI water and sonicated for 10 h using a probe sonicator at 270 W. After the undispersed CNT were removed through centrifugation at 10,000 rpm for 1 h, 10 mg dopamine (DOPA) was added under stirring at 40 °C for 1 h. Next, 10 mL of 0.1 M Tris buffer (pH 7.5) was added into the DOPA-containing CNT dispersion to initialize the polymerization of dopamine. Finally, the PDA-coated CNT dispersion with an overall concentration of 0.18 ± 0.06 mg mL^{-1} was obtained after reaction at 40 °C for 6 h and centrifugation at 10,000 rpm for 30 min.

Fabrication of CNT-supported polyamide (PA) membranes: The CNT-PA membrane was fabricated by forming a PA selective layer on top of a PES-CNT membrane and then removing the PES support via dissolution in dimethylacetamide (DMAc). Specifically, first, a PES-CNT membrane was synthesized via the vacuum filtration of PDA-coated CNT dispersion (with volumes of 0.3, 1.5, 3.0, 4.5 and 6.0 mL, respectively, to obtain different CNT layer thickness) through a PES microfiltration membrane (with pore size of 0.22 μm). The loaded PDA-coated CNT amount on PES was 0.04, 0.21, 0.42, 0.64 and 0.86 g m^{-2}, respectively. Then, a PA layer was formed through interfacial polymerization of 3.4 wt% m-phenylenediamine (MPD) water solution and 0.15 wt% trimesoyl chloride (TMC) hexane solution on the PES-CNT membrane, following a reported protocol [25]. Finally, the PES-CNT-PA membrane was immersed in DMAc solvent for 5 min to etch off the PES support, and the resulting translucent CNT-supported PA membrane (CNT-PA) was transferred into DI water to remove residual DMAc. The CNT-PA membrane was stored in DI water at 4 °C ready for characterization and measurement.

Membrane Test: The water flux J_w and reverse salt flux J_s of CNT-PA membranes were measured in custom-designed FO test systems (Figs. S1 and S2). DI water and 1.0 M NaCl solution were used as the feed and draw solutions, respectively. The NaCl rejection was tested in a reverse osmosis (RO) system (Fig. S3). The membranes were tested in both PRO (active layer facing draw solution, AL-DS) and FO (active layer facing feed solution, AL-FS) operation modes. The water flux was calculated as the water weight gain of the draw solution per hour and per area of the membrane and was measured by taking out the draw solution after 30-min test and using an electric balance (ME3002, Mettler-Toledo, Switzerland). The reverse salt flux was calculated as the salt weight gain of the feed side per hour and per area of the membrane, and was measured using a conductivity meter (CON2700, Eutech, USA) in the feed solution. More details were discussed in supporting information. In the OSFO tests, PEG400 was explored as draw solution, the measurement of solvent flux and reverse solute flux were the same as that of the water/salt system discussed above. The modified Dragendorff approach [32] and UV–Vis were used to detect the concentration of PEG400. The concentration of RhB in a solvent was measured by the UV–Vis spectrophotometer (Shimadzu, UV-2700, Japan).

Characterization: A scanning electron microscope (SEM, S-4800, Hitachi, Japan) was used to observe the surface and cross-sectional morphologies of all membranes with 3 keV energy. Cross-sectional samples were acquired by snapping wet CNT-PA onto silica wafers in liquid nitrogen. All samples were dried in air overnight and coated with platinum (Pt) for 100s using an EMITECH SC7620 sputter coater before SEM imaging. An X-ray photoelectron spectroscope (XPS, Thermo Esca Lab 250Xi, USA) was employed to determine the elemental compositions of polyamide surface of a membrane using a monochromatic Al Kα X-ray source (hv = 1486.6 eV), with XPS peak software for data processing. Atomic force microscopy (AFM, Multi-Mode 8, Veeco, US) was used to observe the membrane surface morphology and measure the membrane surface roughness in tapping mode using TESP tips (Sharp silicon probe, 42 N/m, 320 kHz, tip radius 8 nm, no coating, Bruker, USA). AFM images were processed using Nanoscope Analysis software, and the surface roughness was presented as the average roughness (Ra) from at least three different samples. Water contact angles were measured using the sessile drop method on an optical instrument (OCA20, Data Physics, Germany) at room temperature. Adsorption-branch n-hexane/helium permporometry was used to estimate the distribution of the pore size of CNT membranes with various CNT thickness, according to a reported protocol [33]. The mechanical strength of membrane was measured using a universal mechanical testing machine (HY-0580, Shanghai Hengyi Precision Instruments, Shanghai, China).

For each experiment, at least three individual specimens were measured and an average value with a standard deviation was reported. The grazing-incidence small-angle X-ray scattering (GISAXS, Xeuss 2.0, Xenocs, France) measurement was performed at the beam line at the Institute of Seawater Desalination and Multipurpose Utilization (Tianjin, China) to determine the molecular void or pore size of the polyamide layer on CNT-PA membranes. The incident beam size is 0.7 mm × 0.7 mm and the beam wavelength λ is 1.5405 Å. The grazing angle was 0.2° onto the sample surface. A two-dimensional Pilatus 200 K detector was set at a distance of 0.2.0 M from the sample center to collect the scattering spectra at high momentum transfer vector (Q) value. An acquisition time of 900 s was used for all samples to achieve strong signals.

3. Results and discussion

3.1. Surface and structure of the CNT support

The fabrication procedure of the carbon nanotubes supported polyamide (CNT-PA) membrane is schematically illustrated in Scheme 1. First, a CNT support was prepared via the vacuum filtration of a polydopamine (PDA)-coated single wall CNT dispersion on a PES substrate with 0.22 μm pore size, and then a PA selective layer was synthesized on the porous surface of the CNT support through interfacial polymerization (IP) of m-phenylenediamine (MPD) and trimesoyl chloride (TMC). A free-standing CNT-PA membrane was obtained by subsequently dissolving the PES support in dimethylacetamide (DMAc).

To optimize the structural and transport properties of PA selective layer, CNT supports with various thicknesses were prepared through controlling the deposition amount of the CNT dispersion on the PES substrate as shown in Fig. 1, and their surface properties including morphology, pore size, and hydrophilicity were characterized as list in Table 1. Results illustrate that the surface pores of the PES membrane can be partially covered by CNT network with CNT solution deposition amount of 0.3 mL (PES-CNT-1). Further increasing loading amount of CNT, the CNT support became denser with decreased water flux from 1032 LMH bar^{-1} to 210 LMH bar^{-1} (PES-CNT-5) and their average pore size in diameter decreased from 15.7 ± 1.5 nm to 4.9 ± 0.8 nm (Fig. S4). The water contact angle of the CNT supports increased from 21.4 ± 1.7° (PES-CNT-1) to 35.9 ± 0.5° (PES-CNT-5), which may be due to the decreased pore size from the increasing dense packing of the CNT nanofibers. Additionally, the thickness of CNT support presented a proportional increase from about 100 nm to approximately 400 nm (Table 1), and the roughness of the CNT support decreased from 53.2 ± 4.9 nm to 17.5 ± 2.4 nm with the increasing loading amount of CNT (Fig. 2). Therefore, the CNT support became denser, smoother, and thicker with more loading amount of CNT dispersion on the PES substrate.

3.2. Effects of the CNT support on the formation of polyamide layer

Next, the PA selective layer was formed on top of the CNT supports with various thicknesses through interfacial polymerization of MPD and TMC. After removing the PES support, free-standing CNT-PA membranes were obtained. The surface morphology and structure of the CNT-PA membranes were characterized using SEM (Fig. 3). The fruitful leaf-like features of PA layer with characteristic ridge-and-valley morphologies were observed on top of CNT support, which is similar as the reported polyamide formed on the dense polymeric substrates [34,35]. The morphologies were totally different from typical "nodular" feature of PA formed on the PES support without CNT (**Fig. S5**). This

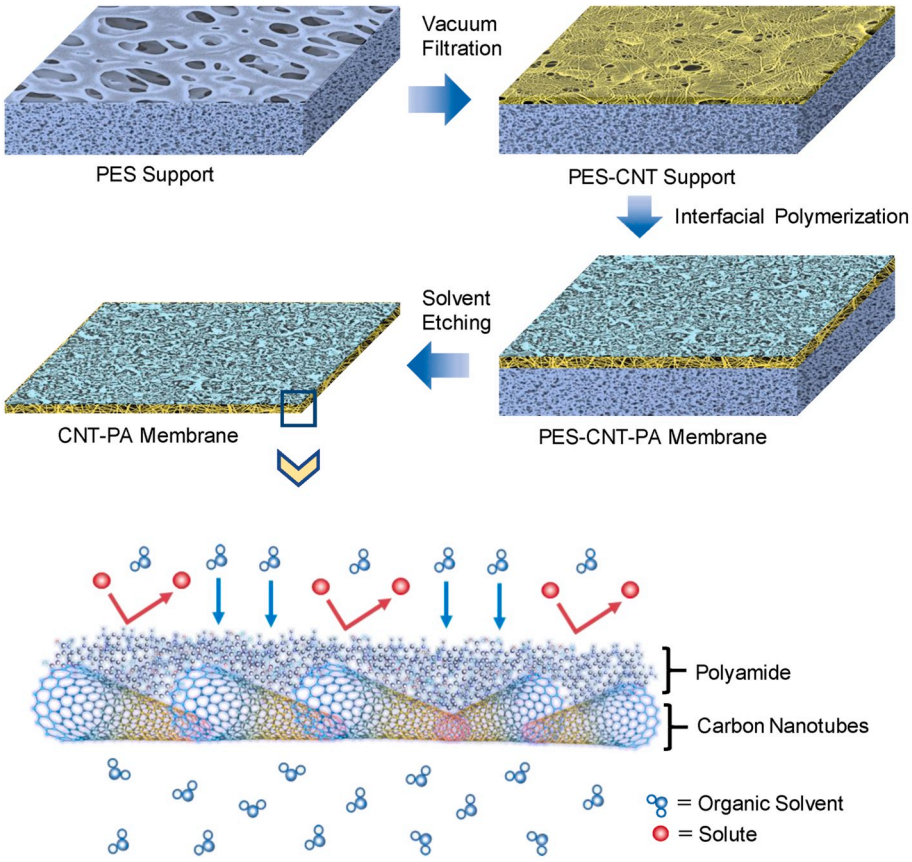

Scheme 1. Schematic illustration of the fabrication process of CNT-PA membrane, including the deposition of CNT on a polyethersulfone (PES) support via vacuum filtration, the polyamide synthesis on top of the CNT-coated PES membrane through interfacial polymerization, and the removal of the PES support by solvent etching.

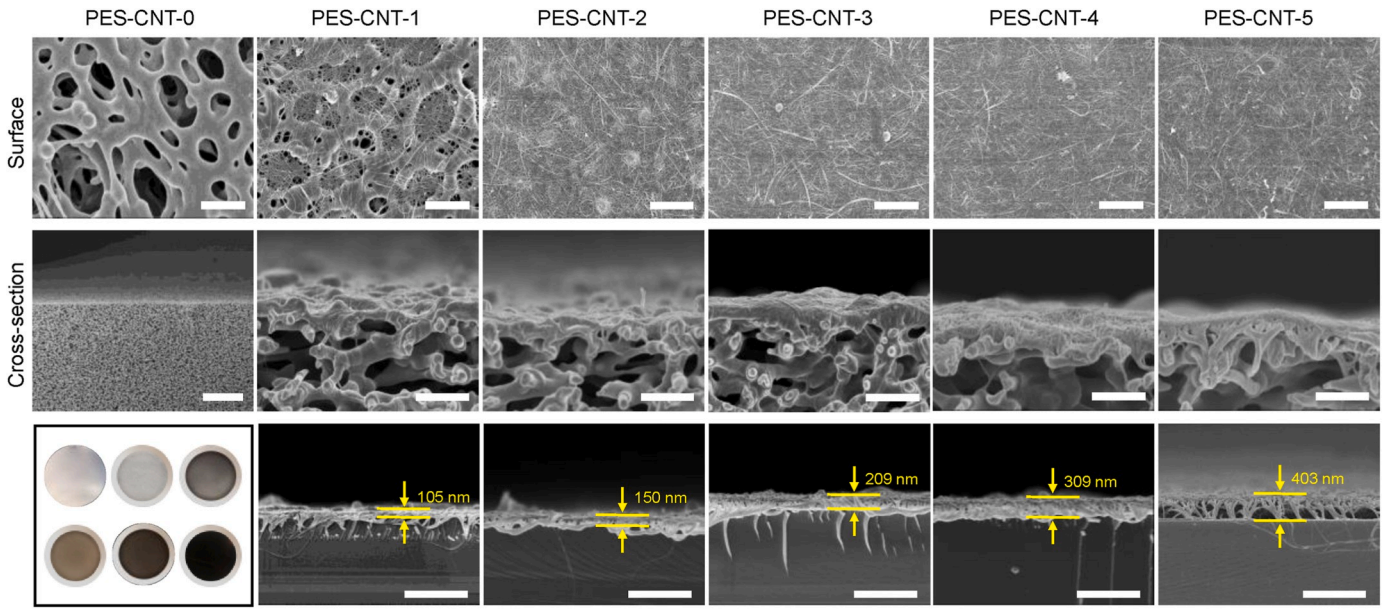

Fig. 1. SEM images of the CNT coated PES supports with various CNT coating amount and the corresponding optical photograph and thickness. (Details provided in Table 1).

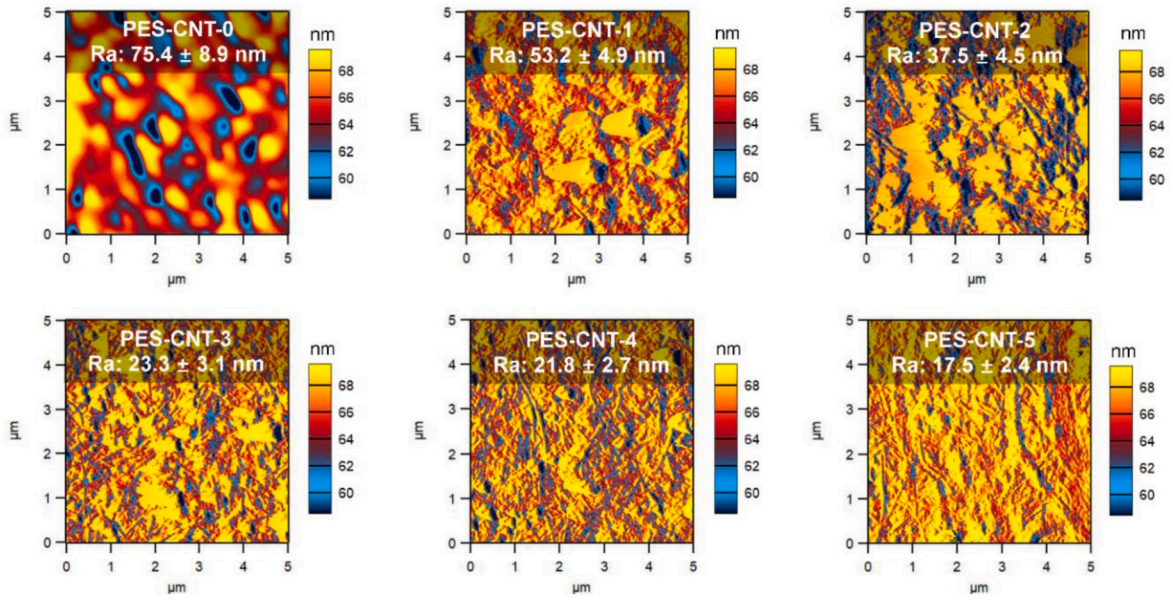

Fig. 2. AFM images of the CNT supports with various thickness of CNT film.

observation has been reported in our previous work [25] that PA with less surface roughness is formed on a hydrophilic substrate with relatively larger pores. The similar result was also reported by many groups [36–38]. The mainly reason is because the diffusion of MPD from aqueous phase to "reaction zone" was limited by the more hydrophilic substrate. Besides, MPD aqueous solution tends to penetrate deep insides the relatively larger pores, thus resulting in typical "nodular" features of PA layer. The SEM images (Fig. 3) of top PA surface of CNT-PA membranes clearly show that the leaf-like features became more in number and larger in size with the increasing CNT support thickness from CNT-PA-1 to CNT-PA-5. And the SEM images of the bottom surface of CNT-PA-1 membrane obviously found that the PA grew inside the CNT support, penetrated from the bottom to the top of CNT support due to its thinner thickness, and covered most of the CNT nanofibers on the back surface. Clear CNT nanofibers with no PA was observed on the back surface of the CNT-PA-3 membranes when the CNT support was 209 ± 11 nm thick or even thicker, suggesting that the PA just grew inside and on the CNT support without penetration into the bottom when the CNT support became thick. Taking CNT-PA-3 as an example, a high-resolution SEM image was shown in Fig. 4. The free-standing membrane showed a typical thin-film-composite structure: CNT bundles at the bottom and the rough polyamide at the top with no clear interface between the CNT and the PA. The membrane was measured using AFM to be 500 nm thick, which is supported by the result from cross-sectional SEM image. The semitransparent membrane exhibited a strong mechanical stability with tensile strength of 14.78 MPa (Fig. S6, S7 and Table S1), which is approximately 3–7 times stronger than traditional polymer membranes [39–41].

AFM images (Fig. 5) obviously present that the height of the PA in the Z-range became taller and the roughness of the PA increased from

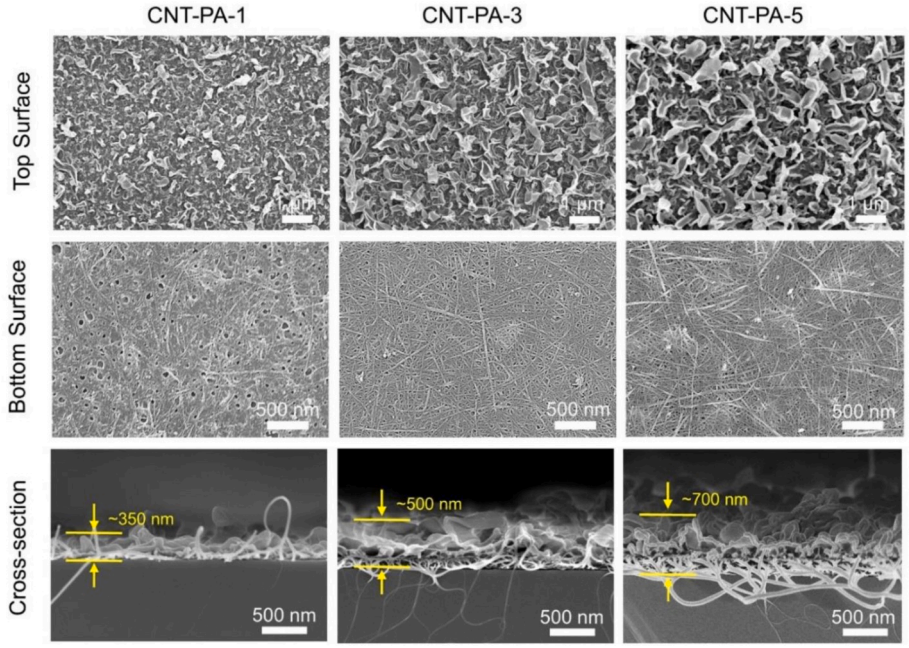

Fig. 3. SEM images including top surface, bottom surface and cross-section morphologies of carbon nanotubes supported polyamide membranes (CNT-PA-1, CNT-PA-3 and CNT-PA-5).

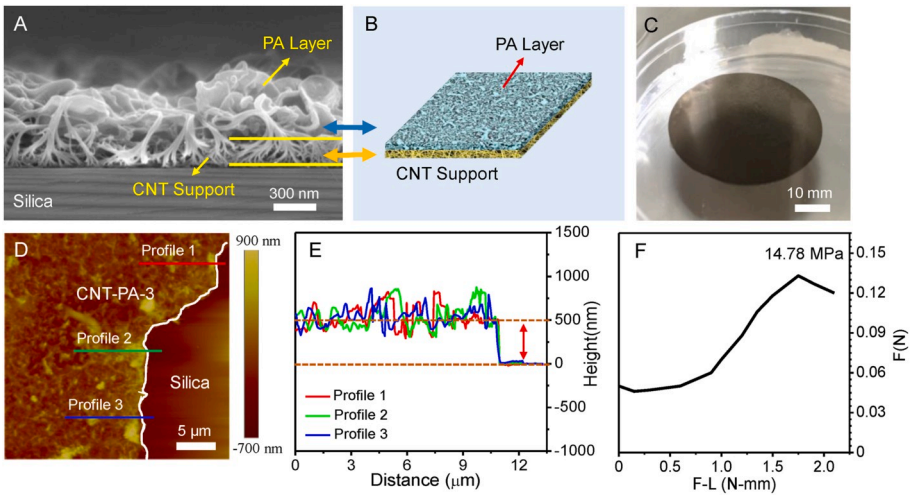

Fig. 4. Characterizations of CNT-PA-3 membrane: cross-sectional SEM image (A), schematic membrane structure (B), optical photograph of CNT-PA-3 (C), large-scale AFM image and corresponding height profile (D and E), and its characteristic tensile-strength curve (F).

108.0 ± 9.9 nm to 134.5 ± 7.9 nm when formed on the thicker CNT support with thickness increasing from 105 ± 8 nm to 403 ± 10 nm. Importantly, the PA surface area ratio was measured using AFM to determine the ratio of total surface area of PA and the projected surface area, and it was significantly increased by 1.55-fold from 2.0 ± 0.2 to 3.1 ± 0.3 when the CNT support thickness increased from 105 ± 8 nm to 209 ± 11 nm, indicating the PA surface area was increased by 1.55-fold (Table 2). To further increase the thickness of CNT support from 209 ± 11 nm to 403 ± 10 nm, the surface area of the formed PA increased slightly within 6%. Since the PA surface area is the effective membrane area proportional to membrane flux, the higher PA surface area brings higher membrane flux [36,42]. Therefore, the surface area of PA formed on the thicker CNT support became larger, which is beneficial to improve membrane flux.

[c] Average pore size of PA is measured through GISAXS and calculated based on the equation $d = 2\pi/Q$, where the momentum transfer (Q, $Q = 4\pi \sin(\theta/2)/\lambda$) is related to scattering angle θ and the wavelength λ [44].

X-ray photoelectron spectroscope (XPS) results illustrate that as the thickness of the CNT support increased, the PA surface became dense with the increasing cross-linking degree from 13.9% to 40.0% (Table 2 and Table S2), confirming more highly cross-linked PA formed on the thicker CNT support. The salt rejections of CNT-PA membranes measured in reverse osmosis operation process showed an obvious increase from 93.82% to 97.29% (Table S3) towards NaCl with the increasing PA cross-linking degree from 13.9% to 40.0%. Grazing-incidence small-angle X-ray scattering (GISAXS) analysis (Table 2 and Fig. S8) illustrates that the pore diameter of PA was 5.01 Å when formed on the 105 ± 8 nm thick CNT support, and decreased slightly to 4.99 Å and 4.92 Å with the increasing cross-linking degree of PA when the thickness of the CNT support became thick to the corresponding 209 ± 11 nm and 403 ± 10 nm. All the results above support well with the fact that PA with the higher cross-linking degree and smaller pore exhibited

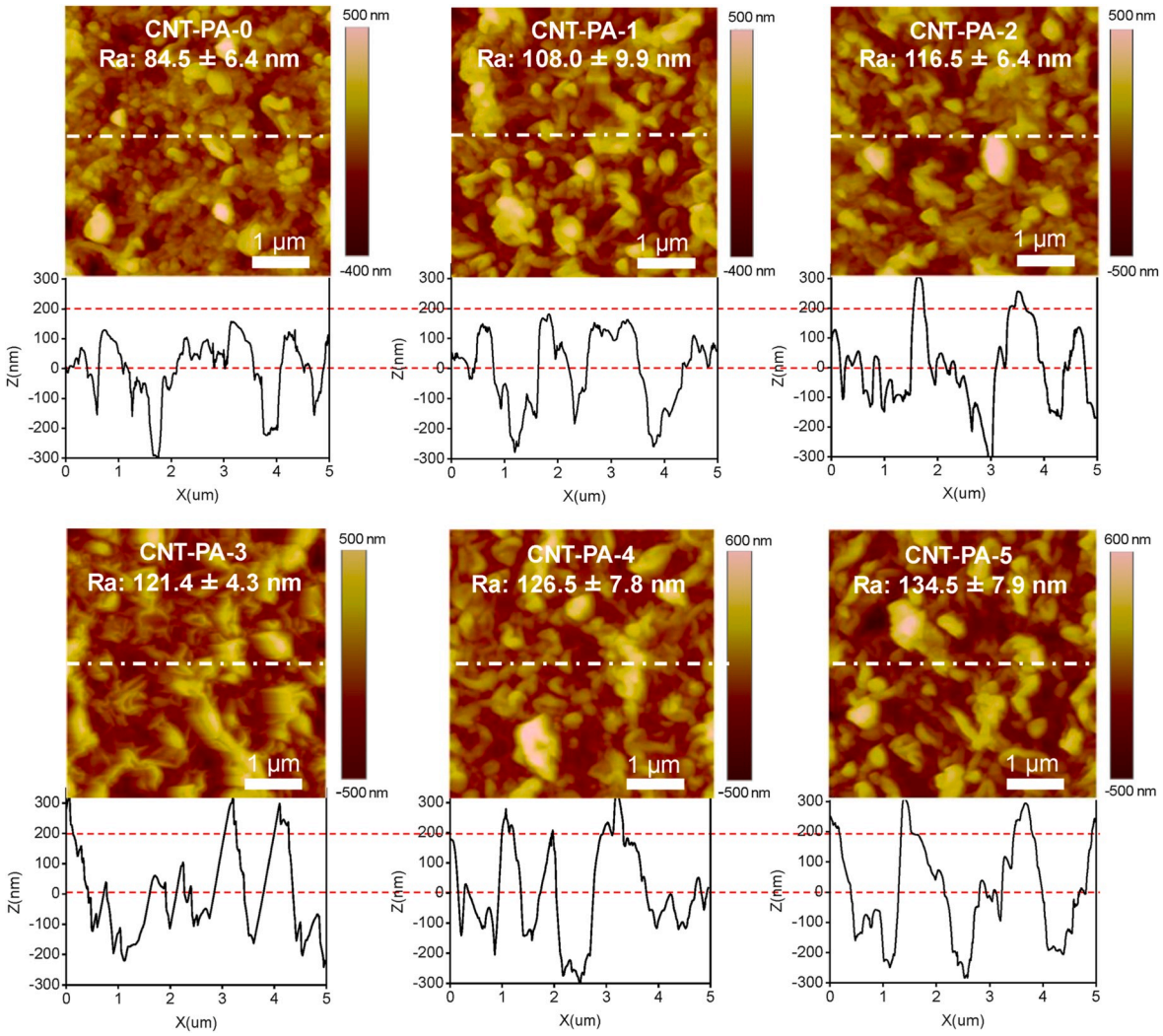

Fig. 5. AFM images of carbon nanotubes supported polyamide membranes with various thickness of CNT support and the corresponding height profile.

Table 1
Characteristic parameters of CNT supports with various thickness.

Membrane	CNT amount [mL]	CNT thickness [nm]	Average pore size [nm]	Roughness [nm]	Surface porosity [%]	Water flux [LMH/bar]	Water contact angle [°]
PES-CNT-0	0.0	0	–	75.4 ± 8.9	19.6	10,280 ± 1290	10.7 ± 1.4
PES-CNT-1	0.3	105 ± 8	15.7 ± 1.5	53.2 ± 4.9	60.7	1032 ± 1065	21.4 ± 1.7
PES-CNT-2	1.5	150 ± 10	8.4 ± 1.3	37.5 ± 4.5	53.6	790 ± 952	25.4 ± 1.4
PES-CNT-3	3.0	209 ± 11	6.0 ± 1.1	23.3 ± 3.1	52.3	532 ± 402	33.5 ± 0.8
PES-CNT-4	4.5	309 ± 13	5.1 ± 0.9	21.8 ± 2.7	51.8	396 ± 396	34.3 ± 0.8
PES-CNT-5	6.0	403 ± 10	4.9 ± 0.8	17.5 ± 2.4	51.3	210 ± 93	35.9 ± 0.5

the higher NaCl rejection.

Here, the formation of an increased area of PA layer with higher cross-linking degree on thicker CNT support can be explained from three perspectives: MPD amount on the interface, MPD diffusion and the "heat" generated during the formation of PA. Firstly, the thicker CNT support has a denser packing of CNT nanofibers with a smaller pore size. The pore size of the CNT supports decreased greatly from 15.7 ± 1.5 nm to 4.9 ± 0.8 nm with increased thickness from 105 ± 8 nm to 403 ± 10 nm as listed in Table 1. The thick porous CNT supports hold more MPD solution on its surface, allowed less penetration of the MPD solution into the deep side of the support, leading to a relatively larger MPD amount on the interface [27,45], which promoted the reaction and generated a rougher and more cross-linked PA layer. Secondly, as evidenced in the reported literature [36–38], the rougher PA structure is also probably because of the heterogeneous diffusion of the MPD molecules that are limited by the smaller surface pore size. Besedes, the heat generated during the formation of PA through interfacial polymerization could not dissipate efficiently in the denser packing of CNT support, which then

Table 2
Characteristic parameters of CNT-PA membranes with various thickness of CNT support.

FO membrane	Total thickness [nm]	CNT thickness [nm]	PA thickness [nm]	PA surface area ratio[a]	PA roughness [nm]	Cross-linking degree[b] [%]	PA pore size[c] [Å]
CNT-PA-1	347 ± 31	105 ± 8	269 ± 32	2.0 ± 0.2	108.0 ± 9.9	13.9%	5.01
CNT-PA-2	460 ± 22	150 ± 10	310 ± 24	2.2 ± 0.2	116.5 ± 6.4	26.3%	–
CNT-PA-3	513 ± 18	209 ± 11	304 ± 21	3.1 ± 0.3	121.4 ± 4.3	35.1%	4.99
CNT-PA-4	634 ± 30	309 ± 13	325 ± 33	3.2 ± 0.3	126.5 ± 7.8	37.3%	–
CNT-PA-5	720 ± 54	403 ± 10	317 ± 55	3.3 ± 0.3	134.5 ± 7.9	40.0%	4.92

[a] PA surface area ratio is measured using AFM to determine the ratio of total surface area of PA and the projected surface area.
[b] Cross-linking degree of PA is measured by XPS and calculated following the reported method [43].

increased the local temperature and also increased the interfacial instability to form a rougher PA with a larger surface area. This observation is consistent with the report by Livingston et al. [36] who provided a possible growth mechanism of polyamide with crumpled structures based on heat generation in the interfacial reaction.

3.3. Evaluation of the internal concentration polarization of the CNT-PA membranes in aqueous solution

Water and salt transport properties of the fabricated CNT-PA membranes were measured to investigate and evaluate the FO performance and ICP effect using DI water as feed solution and NaCl solution as draw solution. First, the effect of the CNT supports with various thickness on water/salt FO performance was investigated. Results reveal that, as the CNT support thickness increased, the water flux of CNT-PA membranes increased first and then decreased (Fig. 6A), which is ascribed to the balance of the increased water permeability of PA with larger surface area and the increased water transport resistance from more highly cross-linked PA formed on the thicker CNT support and also the relatively severer ICP from the thicker CNT support itself. In comparison, as the CNT support thickness increased, the reverse salt flux of CNT-PA membranes decreased dramatically from over 150 g m^{-2} h^{-1} (CNT-PA-1) to approximately 50 g m^{-2} h^{-1} (CNT-PA-3) due to the increased PA thickness (from 269 ± 32 nm to 304 ± 21 nm), increased cross-linking degree, and decreased pore sizes of the polyamide layer. The reverse salt flux of the membranes from CNT-PA-3 to CNT-PA-5 is fluctuant in the range of 50–60 g m^{-2} h^{-1}, which should attribute to their similar PA thickness and cross-linking degree. CNT-PA-3 exhibited the highest water flux of 139.05 ± 5.23 when tested in the FO mode (over 150 LMH in PRO) using DI water as a feed solution and 1.0 M NaCl as a draw solution. As shown in Fig. 5B, the water flux of CNT-PA-3 is 686% higher than that of commercial HTI TFC-ES FO membrane (17.70 ± 3.3 LMH under the same test conditions), and about 3 times higher than those of 100-nm-thick rGO membranes and 4–10 times [46] than

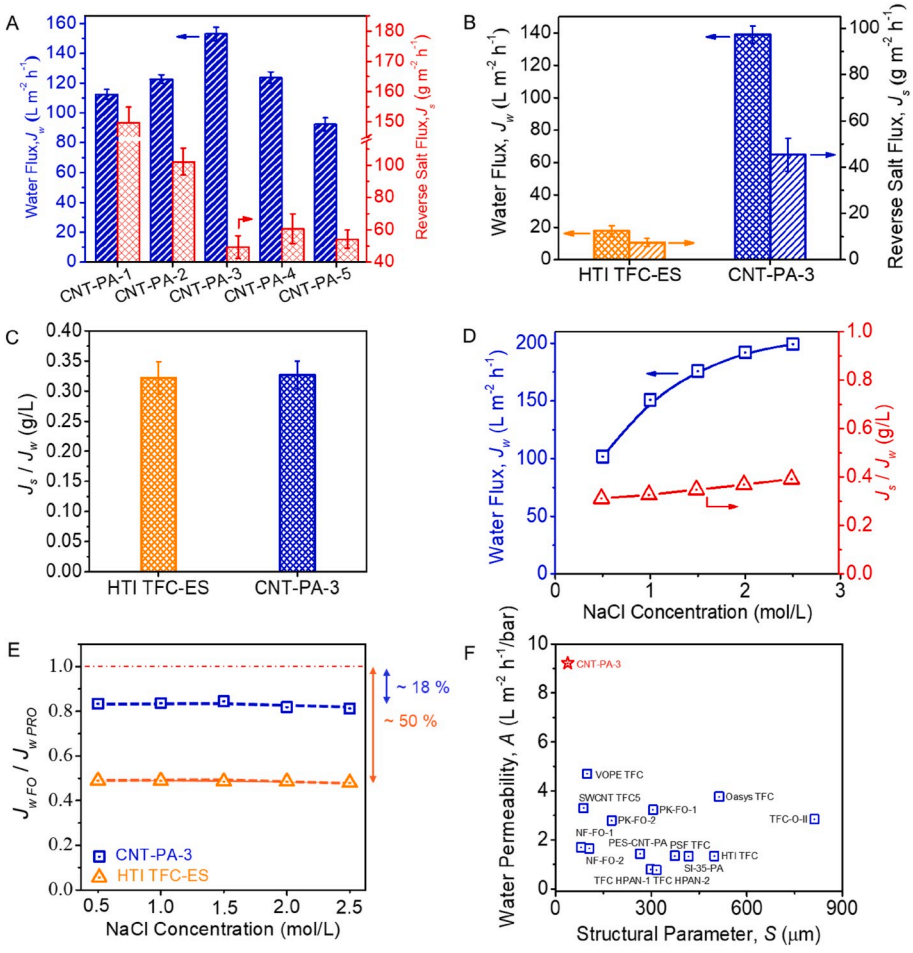

Fig. 6. Water and salt transport properties of CNT-PA membranes as a comparison with the commercialized TFC FO membrane: water flux and reverse salt flux measured in the PRO mode (A and B), using DI water as a feed solution and 1.0 M NaCl as a draw solution; specific salt flux (J_s/J_w) of the prepared CNT-PA-3 membrane and the commercialized TFC FO membrane (C), water flux and specific salt flux (J_s/J_w) of the prepared CNT-PA-3 membrane as a function of draw solution concentrations (D), water flux ratio of $J_{w\,FO}$ to $J_{w\,PRO}$ as a function of draw solution concentrations (E); and water permeability coefficient A and structure parameter S of the CNT-PA-3 membrane in this work and in literature (F), using data from Table S4.

those the lab-made TFC-FO membranes [47–49]. The apparent reverse salt flux of the CNT-PA-3 membrane is obviously higher than that of commercial HTI TFC-ES FO membrane (Fig. 6B). While, the specific salt flux (reverse salt flux over water flux, J_s/J_w) [50] of CNT-PA-3 is 0.327 ± 0.023 g/L, comparable with 0.322 ± 0.027 g/L of the commercial HTI TFC-ES FO membrane under the same test conditions (Fig. 6C). It reveals the good selectivity of the CNT-PA-3 membrane. Besides, the prepared CNT-PA-3 membrane showed a relative stable specific salt flux (slightly increase from 0.322 g/L to approximately 0.4 g/L) (Fig. 6D) under various NaCl concentrations, indicating that the membrane selectivity can be well preserved. Based on the excellent permeability and selectivity, CNT-PA-3 membrane was used as the best-performance membrane for further ICP evaluation.

The water flux ratio $J_{w\ FO}/J_{w\ PRO}$ at the two orientations is an indicator of ICP. Higher water flux ratios indicate lower ICP [23]. The commercial HTI TFC-ES FO membrane exhibited a much lower water flux ratio around 0.5, due to a severe diffusive barrier in the tortuous polymeric support layers. Excitingly, CNT-PA-3 membrane had a water flux ratio of $J_{w\ FO}/J_{w\ PRO}$ in the range of 0.81–0.85 with various draw solution concentrations, as shown in Fig. 6E, showing the significantly suppressed ICP of the CNT support in comparison to the conventional phase-inversion polymeric support.

The structural parameter S, pure water permeability coefficient A and solute permeability coefficient B offer universal benchmark for comparing membrane performance, regardless of operating condition [51]. FO performance of our CNT-PA-3 membrane in the aspect of structural parameter S and water permeability coefficient A, were compared with those of the reported FO membranes and commercial membranes, as shown in Fig. 6F. The S value of CNT-PA membranes was 38 ± 12 μm, which is much lower than that of the most reported FO membranes, showing that the CNT support significantly reduced the water transport length and thus resistance. The decreased S value also indicated that the greatly decreased ICP of the CNT support has a direct relation between S and IPC [52]. The A value of the CNT-PA-3 membrane was 9.22 ± 1.14 LMH·bar^{-1}, the highest A among the reported TFC FO membranes to our best knowledge (Table S4), resulting from both the increased effective area of PA layer for more water permeation and less water transport resistance from the ultrathin porous CNT support.

3.4. Organic solvent forward osmosis performance

Organic solvent transport properties of the CNT-PA membrane were tested in the forward osmosis process using 2.0 M PEG400 in several organic solvents as draw solutions and using the corresponding solvents as feed solutions (Scheme 2). Benefitting from the highly permeable PA and the ultrathin CNT support, the CNT-PA membrane exhibited quite high solvent fluxes for DMAc (20.78 LMH), DMF (19.79 LMH), DMSO (13.50 LMH) and EtOH (2.83 LMH) as shown in Fig. 7A. The transport of solvents through PA layer is typically described by the solution-diffusion theory. The solubility parameter δ, the molar diameter d and solvent viscosity η have greatly influence on membrane performance. Specifically, there is a linear correlation between the permeance and molecular properties $\left(\frac{\delta}{\eta d^2}\right)$, which is a typical transport feature of polyamide membrane reported in previous works [36,45]. The DMAc and DMF solvent fluxes of the CNT-PA membrane are higher than that of DMSO and EtOH, which is mainly because of the similar Hansen solubility parameter [53] of DMAc (22.7 MPa$^{1/2}$) and DMF (24.8 MPa $^{1/2}$) as the polyamide (23 MPa$^{1/2}$) selective layer resulting in the fast transport of solvents. Additionally, although EtOH (26.7 MPa$^{1/2}$) has a Hansen similar solubility parameter with DMSO (26.6 MPa$^{1/2}$), but has a lower viscosity (1.17 mPa s of EtOH vs. 1.99 mPa s of DMSO) and a smaller molar diameter (0.57 nm of EtOH vs. 0.61 nm of DMSO), the EtOH flux of the CNT-PA membrane is much lower than that of DMSO. This is because DMSO is a better swelling solvent for aromatic polyamides than

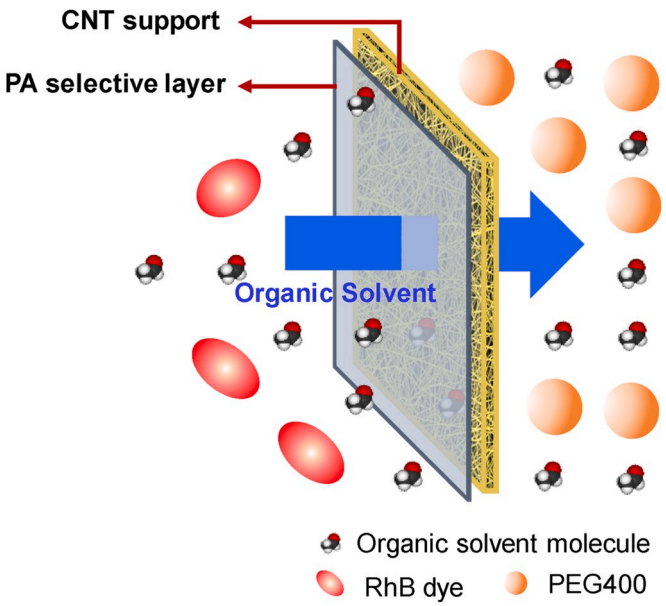

Scheme 2. Schematic diagram of the OSFO process.

EtOH in terms of solubility parameter due to the dispersion force and hydrogen bonding [53]. Note that the osmotic pressure and mass transfer mechanism in OSFO systems were not fully understood yet, and needed further investigation as a separated work. Importantly, the reverse PEG400 flux is zero, since PEG400 could not be detected in all four feed solutions even after a 12-h testing. The results confirm that the CNT-PA membrane performed stably as a selective membrane in organic solvents such as DMAc, DMF, DMSO and EtOH.

To better evaluate the real application of the CNT-PA membrane in the OSFO process for organic solvent recovery, Rhodamine B (RhB) was introduced as a model organic molecule into the above-mentioned four organic solvents as feed solutions. Fig. 7B presents that the CNT-PA membrane exhibited a near 100% rejection towards the RhB dye in these four organic solvents during the 12-h testing (Fig. S12, **S13**). The solvent fluxes here showed a slight decrease compared with the pure solvent fluxes, for example, the flux of DMAc decreased from 20.78 LMH to 18.21 LMH after adding RhB in the feed solution. It is mainly because of the potential membrane fouling from RhB in the feed solution. It is worth mentioning that the CNT-PA membrane showed great mechanical stability in organic solvents. PA layer and the CNT support did not peel off from each other even immersing the membrane in 80 °C DMF for 4 weeks and no structures damages were observed from SEM images after OSFO tests. Therefore, it can conclude that the CNT-PA membrane has a great potential to be applied in the concentration of chemicals and the recovery of organic solvents through the forward osmosis process.

4. Conclusions

In conclusion, we have successfully replaced the conventional polymeric support by CNT network in the fabrication of TFC membranes. Results demonstrate that the CNT support provides a favorable surface to fabricate highly permeable PA selective layer, and also exhibits a highly porous structure to enable water and organic solvents to pass through the entire PA layer surface. Besides, the CNT network works as an ultrathin support with a low tortuosity to decrease the structure parameter S of the fabricated CNT-PA membrane, and to also decrease the transport resistance with the reduced ICP effect. As a result, the CNT-PA-3 membrane achieved the super high water flux of 150 LMH when using 1.0 M NaCl as draw solution and DI water as feed solution. More importantly, the prepared CNT-PA membrane was used in the OSFO process for organic solvent recovery. The CNT-PA-3 membrane

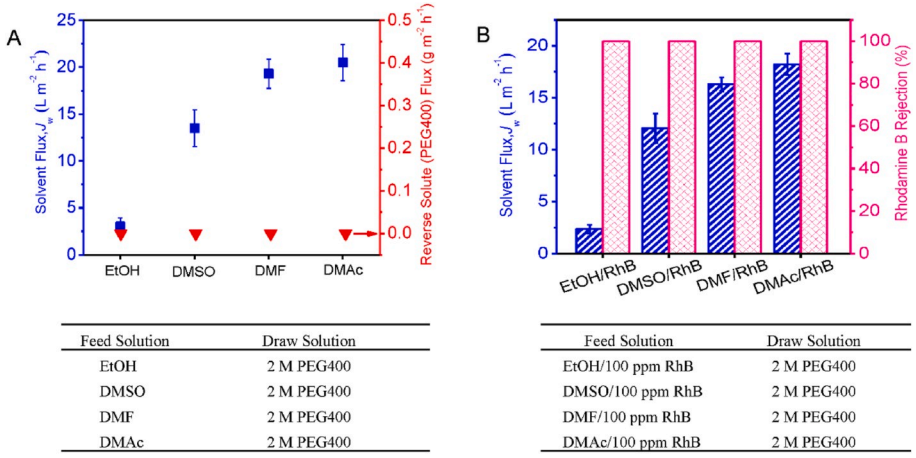

Feed Solution	Draw Solution
EtOH	2 M PEG400
DMSO	2 M PEG400
DMF	2 M PEG400
DMAc	2 M PEG400

Feed Solution	Draw Solution
EtOH/100 ppm RhB	2 M PEG400
DMSO/100 ppm RhB	2 M PEG400
DMF/100 ppm RhB	2 M PEG400
DMAc/100 ppm RhB	2 M PEG400

Fig. 7. Various solvents transport properties of the CNT-PA membrane (the CNT-PA-3 membrane was used) when measured in the FO mode, using RhB containing organic solution as a feed solution and 2.0 M PEG400 in an organic solvent as a draw solution. Four representative organic solvents were selected including ethanol (EtOH), dimethylsulfoxide (DMSO), dimethylformamide (DMF) and dimethylacetamide (DMAc).

gave the DMAc flux of 20.78 LMH and near zero reverse solute flux when using 2.0 M PEG400 as draw solute and pure DMAc as the feed solution. The CNT-PA membrane also showed a great capability to recover DMSO, DMF and DMAc in the OSFO process and to concentrate organic molecules in the feed solutions simultaneously. Further study is needed to purify solvents and to regenerate the draw solutes like the aqueous FO system. All the results showed that the CNT-supported PA membrane has great potential in both aqueous FO process and OSFO applications with significantly reduced ICP and strong solvent resistant.

Author contribution

Zongyao Zhou contributed to majority of the experiment and data analysis. Qun Wang helped in the data analysis. Baoxia Mi helped in editing the manuscript. The original draft was prepared by Zongyao Zhou, and reviewed, validated, and edited by Yunxia Hu.

Declaration of competing interest

The authors declare that they have no known competing financial interests or personal relationships that could have appeared to influence the work reported in this paper.

Acknowledgements

The authors gratefully acknowledge the funding support from National Natural Science Foundation of China (No.21476249, No.21978215), Chang-jiang Scholars and Innovative Research Team in the University of Ministry of Education, China (No. IRT-17R80) and the Science and Technology program of Tianjin (No.18JCZDJC37100). B.M. acknowledges the support from the U.S. National Science Foundation under award nos. CBET-1565452 and CBET-1706059.

Appendix A. Supplementary data

Supplementary data to this article can be found online at https://doi.org/10.1016/j.memsci.2020.118273.

References

[1] D. Emadzadeh, W.J. Lau, T. Matsuura, M. Rahbari-Sisakht, A.F. Ismail, A novel thin film composite forward osmosis membrane prepared from PSf–TiO2 nanocomposite substrate for water desalination, Chem. Eng. J. 237 (2014) 70–80.
[2] G. Han, T.-S. Chung, M. Toriida, S. Tamai, Thin-film composite forward osmosis membranes with novel hydrophilic supports for desalination, J. Membr. Sci. 423 (2012) 543–555.
[3] J.R. McCutcheon, R.L. McGinnis, M. Elimelech, A novel ammonia—carbon dioxide forward (direct) osmosis desalination process, Desalination 174 (2005) 1–11.
[4] Y.-N. Wang, K. Goh, X. Li, L. Setiawan, R. Wang, Membranes and processes for forward osmosis-based desalination: recent advances and future prospects, Desalination 434 (2018) 81–99.
[5] L. Shen, X. Zhang, L. Tian, Z. Li, C. Ding, M. Yi, C. Han, X. Yu, Y. Wang, Constructing substrate of low structural parameter by salt induction for high-performance TFC-FO membranes, J. Membr. Sci. 600 (2020), 117866.
[6] X. An, Y. Hu, N. Wang, Z. Zhou, Z. Liu, Continuous juice concentration by integrating forward osmosis with membrane distillation using potassium sorbate preservative as a draw solute, J. Membr. Sci. 573 (2019) 192–199.
[7] D.I. Kim, G. Gwak, M. Zhan, S. Hong, Sustainable dewatering of grapefruit juice through forward osmosis: improving membrane performance, fouling control, and product quality, J. Membr. Sci. 578 (2019) 53–60.
[8] S. Xiong, S. Xu, S. Zhang, A. Phommachanh, Y. Wang, Highly permeable and antifouling TFC FO membrane prepared with CD-EDA monomer for protein enrichment, J. Membr. Sci. 572 (2019) 281–290.
[9] Q. Ge, P. Wang, C. Wan, T.-S. Chung, Polyelectrolyte-promoted forward osmosis–membrane distillation (FO–MD) hybrid process for dye wastewater treatment, Environ. Sci. Technol. 46 (2012) 6236–6243.
[10] K.L. Hickenbottom, N.T. Hancock, N.R. Hutchings, E.W. Appleton, E.G. Beaudry, P. Xu, T.Y. Cath, Forward osmosis treatment of drilling mud and fracturing wastewater from oil and gas operations, Desalination 312 (2013) 60–66.
[11] R.P. Lively, D.S. Sholl, From water to organics in membrane separations, Nat. Mater. 16 (2017) 276.
[12] Y. Cui, T.-S. Chung, Pharmaceutical concentration using organic solvent forward osmosis for solvent recovery, Nat. Commun. 9 (2018) 1426.
[13] A. Aliprandi, D. Pakulski, A. Ciesielski, P. Samorì, Punctured two-dimensional sheets for harvesting blue energy, ACS Nano 11 (2017) 10654–10658.
[14] J.R. McCutcheon, R.L. McGinnis, M. Elimelech, Desalination by ammonia–carbon dioxide forward osmosis: influence of draw and feed solution concentrations on process performance, J. Membr. Sci. 278 (2006) 114–123.
[15] T.Y. Cath, A.E. Childress, M. Elimelech, Forward osmosis: principles, applications, and recent developments, J. Membr. Sci. 281 (2006) 70–87.
[16] M.J. Park, S. Phuntsho, T. He, G.M. Nisola, L.D. Tijing, X.-M. Li, G. Chen, W.-J. Chung, H.K. Shon, Graphene oxide incorporated polysulfone substrate for the fabrication of flat-sheet thin-film composite forward osmosis membranes, J. Membr. Sci. 493 (2015) 496–507.
[17] M.A. Shannon, P.W. Bohn, M. Elimelech, J.G. Georgiadis, B.J. Marinas, A. M. Mayes, Science and technology for water purification in the coming decades. Nanoscience and Technology: a Collection of Reviews from Nature Journals, World Scientific, 2010, pp. 337–346.
[18] A. Subramani, J.G. Jacangelo, Emerging desalination technologies for water treatment: a critical review, Water Res. 75 (2015) 164–187.
[19] S. Zhao, L. Zou, Relating solution physicochemical properties to internal concentration polarization in forward osmosis, J. Membr. Sci. 379 (2011) 459–467.
[20] N. Ma, J. Wei, S. Qi, Y. Zhao, Y. Gao, C.Y. Tang, Nanocomposite substrates for controlling internal concentration polarization in forward osmosis membranes, J. Membr. Sci. 441 (2013) 54–62.
[21] S. Zhang, K.Y. Wang, T.-S. Chung, H. Chen, Y. Jean, G. Amy, Well-constructed cellulose acetate membranes for forward osmosis: minimized internal concentration polarization with an ultra-thin selective layer, J. Membr. Sci. 360 (2010) 522–535.
[22] G.T. Gray, J.R. McCutcheon, M. Elimelech, Internal concentration polarization in forward osmosis: role of membrane orientation, Desalination 197 (2006) 1–8.

[23] X. Song, Z. Liu, D.D. Sun, Nano gives the answer: breaking the bottleneck of internal concentration polarization with a nanofiber composite forward osmosis membrane for a high water production rate, Adv. Mater. 23 (2011) 3256–3260.
[24] Y. Gao, Y.-N. Wang, W. Li, C.Y. Tang, Characterization of internal and external concentration polarizations during forward osmosis processes, Desalination 338 (2014) 65–73.
[25] Z. Zhou, Y. Hu, C. Boo, Z. Liu, J. Li, L. Deng, X. An, High-performance thin-film composite membrane with an ultrathin spray-coated carbon nanotube interlayer, Environ. Sci. Technol. Lett. 5 (2018) 243–248.
[26] N. Widjojo, T.-S. Chung, M. Weber, C. Maletzko, V. Warzelhan, The role of sulphonated polymer and macrovoid-free structure in the support layer for thin-film composite (TFC) forward osmosis (FO) membranes, J. Membr. Sci. 383 (2011) 214–223.
[27] G. Gong, P. Wang, Z. Zhou, Y. Hu, New insights into the role of an interlayer for the fabrication of highly selective and permeable thin-film composite nanofiltration membrane, ACS Appl. Mater. Interfaces 11 (2019) 7349–7356.
[28] Z. Jiang, S. Karan, A.G. Livingston, Water transport through ultrathin polyamide nanofilms used for reverse osmosis, Adv. Mater. 30 (2018) 1705973.
[29] H.-Q. Liang, W.-S. Hung, H.-H. Yu, C.-C. Hu, K.-R. Lee, J.-Y. Lai, Z.-K. Xu, Forward osmosis membranes with unprecedented water flux, J. Membr. Sci. 529 (2017) 47–54.
[30] B.E. Logan, M. Elimelech, Membrane-based processes for sustainable power generation using water, Nature 488 (2012) 313.
[31] Y. Zhu, W. Xie, S. Gao, F. Zhang, W. Zhang, Z. Liu, J. Jin, Single-walled carbon nanotube film supported nanofiltration membrane with a nearly 10 nm thick polyamide selective layer for high-flux and high-rejection desalination, Small 12 (2016) 5034–5041.
[32] Z. Jia, C. Tian, Quantitative determination of polyethylene glycol with modified Dragendorff reagent method, Desalination 247 (2009) 423–429.
[33] J. Hedlund, D. Korelskiy, L. Sandström, J. Lindmark, Permporometry analysis of zeolite membranes, J. Membr. Sci. 345 (2009) 276–287.
[34] K.Y. Wang, T.-S. Chung, G. Amy, Developing thin-film-composite forward osmosis membranes on the PES/SPSf substrate through interfacial polymerization, AIChE J. 58 (2012) 770–781.
[35] G. Han, S. Zhang, X. Li, N. Widjojo, T.-S. Chung, Thin film composite forward osmosis membranes based on polydopamine modified polysulfone substrates with enhancements in both water flux and salt rejection, Chem. Eng. Sci. 80 (2012) 219–231.
[36] S. Karan, Z. Jiang, A.G. Livingston, Sub–10 nm polyamide nanofilms with ultrafast solvent transport for molecular separation, Science 348 (2015) 1347–1351.
[37] N. Misdan, W. Lau, A. Ismail, T. Matsuura, Formation of thin film composite nanofiltration membrane: effect of polysulfone substrate characteristics, Desalination 329 (2013) 9–18.
[38] P.S. Singh, S. Joshi, J. Trivedi, C. Devmurari, A.P. Rao, P. Ghosh, Probing the structural variations of thin film composite RO membranes obtained by coating polyamide over polysulfone membranes of different pore dimensions, J. Membr. Sci. 278 (2006) 19–25.
[39] X. Yu, F. Liu, L. Wang, Z. Xiong, Y. Wang, Robust poly(lactic acid) membranes improved by polysulfone-g-poly(lactic acid) copolymers for hemodialysis, RSC Adv. 5 (2015) 78306–78314.
[40] Y.C. Xu, Y.P. Tang, L.F. Liu, Z.H. Guo, L. Shao, Nanocomposite organic solvent nanofiltration membranes by a highly-efficient mussel-inspired co-deposition strategy, J. Membr. Sci. 526 (2017) 32–42.
[41] A. Abdel-Karim, T.A. Gad-Allah, A.S. El-Kalliny, S.I.A. Ahmed, E.R. Souaya, M. I. Badawy, M. Ulbricht, Fabrication of modified polyethersulfone membranes for wastewater treatment by submerged membrane bioreactor, Separ. Purif. Technol. 175 (2017) 36–46.
[42] Z. Wang, Z. Wang, S. Lin, H. Jin, S. Gao, Y. Zhu, J. Jin, Nanoparticle-templated nanofiltration membranes for ultrahigh performance desalination, Nat. Commun. 9 (2018) 2004.
[43] B. Khorshidi, T. Thundat, B.A. Fleck, M. Sadrzadeh, A novel approach toward fabrication of high performance thin film composite polyamide membranes, Sci. Rep. 6 (2016) 22069.
[44] J.R. L, J.B. C, Y.W. C, P. Georgopoulos, Grazing-incidence small-angle X-ray scattering: new tool for studying thin film growth, J. Appl. Crystallogr. 22 (1989) 528–532.
[45] Z. Zhou, D. Lu, X. Li, L.M. Rehman, A. Roy, Z. Lai, Fabrication of highly permeable polyamide membranes with large “leaf-like” surface nanostructures on inorganic supports for organic solvent nanofiltration, J. Membr. Sci. 601 (2020), 117932.
[46] H. Liu, H. Wang, X. Zhang, Facile fabrication of freestanding ultrathin reduced graphene oxide membranes for water purification, Adv. Mater. 27 (2015) 249–254.
[47] P. Xiao, L.D. Nghiem, Y. Yin, X.-M. Li, M. Zhang, G. Chen, J. Song, T. He, A sacrificial-layer approach to fabricate polysulfone support for forward osmosis thin-film composite membranes with reduced internal concentration polarisation, J. Membr. Sci. 481 (2015) 106–114.
[48] P.H. Duong, S. Chisca, P.-Y. Hong, H. Cheng, S.P. Nunes, T.-S. Chung, Hydroxyl functionalized polytriazole-co-polyoxadiazole as substrates for forward osmosis membranes, ACS Appl. Mater. Interfaces 7 (2015) 3960–3973.
[49] J. Ren, J.R. McCutcheon, A new commercial thin film composite membrane for forward osmosis, Desalination 343 (2014) 187–193.
[50] M.-t. Tsai, L.-h. Chung, G.-y. Lin, M.-c. Chang, C.-y. Lee, N.-h. Tai, Layered carbon nanotube/polyacrylonitrile thin-film composite membrane for forward osmosis application, Separ. Purif. Technol. 241 (2020), 116683.
[51] A. Tiraferri, N.Y. Yip, A.P. Straub, S.R.-V. Castrillon, M. Elimelech, A method for the simultaneous determination of transport and structural parameters of forward osmosis membranes, J. Membr. Sci. 444 (2013) 523–538.
[52] D.L. Shaffer, J.R. Werber, H. Jaramillo, S. Lin, M. Elimelech, Forward osmosis: where are we now? Desalination 356 (2015) 271–284.
[53] S.M. Aharoni, The solubility parameters of aromatic polyamides, J. Appl. Polym. Sci. 45 (1992) 813–817.